

Activating Antitumor Immunity and Antimetastatic Effect Through Polydopamine-Encapsulated Core–Shell Upconversion Nanoparticles

Shuangqian Yan, Xuemei Zeng, Yong'an Tang, Bi-Feng Liu,* Yu Wang,*
and Xiaogang Liu*

Synergistic phototherapy has the potential to conquer the extreme heterogeneity and complexity of difficult tumors and result in better cancer treatment outcomes than monomodal photodynamic therapy (PDT) or photothermal therapy (PTT). However, the previous approaches to combining PDT and PTT are mainly focused on primary tumor obliteration while neglecting tumor metastasis, which is responsible for about 90% of cancer deaths. It is shown that a combined PDT/PTT approach, based on upconversion-polymer hybrid nanoparticles with surface-loaded chlorin e6 photosensitizer, can enhance primary tumor elimination and elicit antitumor immunity against disseminated tumors. The specific arrangement of an external upconversion coating over the polymer core ensures adequate photoabsorption by the upconversion nanoparticles for the generation of reactive oxygen species upon single near-infrared light irradiation. Furthermore, it is found that synergistic phototherapy can elicit robust systemic and humoral antitumor immune responses. When combined with immune checkpoint blockades, it can inhibit tumor relapse and metastasis as well as prolong the survival of tumor-bearing mice in two types of tumor metastasis models. This study may establish a new modality for enhancing immunogenic cell death through a synergistic phototherapeutic nanoplatform and extend this strategy to overcome tumor metastasis with an augmented antitumor immune response.

Among many forms of multimodal therapies, the combination of photodynamic therapy (PDT) and photothermal therapy (PTT) provides a promising strategy to ablate tumors, while keeping side effects at a minimum.^[4–6]


Owing to their outstanding properties, upconversion nanoparticles (UCNPs) have found critical applications in a variety of biomedical fields, including multimodal imaging, controllable drug delivery, deep-tissue optogenetics, and localized PDT.^[7–18] PDT can induce immunogenic cell death and activate an adaptive immune response against tumor-associated antigens.^[19–28] In addition, the PDT-induced calreticulin, expressed on the surface of immunogenic dying tumor cells, provides an “eat-me” signal for dendritic cell uptake and triggers the response of antitumor immunity.^[29] Similarly, PTT can also generate tumor-associated antigens through tumor treatment and incite the immune responses.^[30–34] For this reason, we reason that UCNPs together with PDT and PTT modalities may provide a powerful toolbox to control antitumor immunity through collaborative effects.^[35]

Combination therapy, based on the use of two or more types of therapies in sequence or at the same time, may offer a solution for cancer treatment because of the synergistic enhancement in the effectiveness of the therapies when in combination.^[1–3]

To validate our hypothesis, we prepared polydopamine (PDA) nanoparticles and coated them with an upconversion layer of NaGdF₄:Yb/Er shell using a coprecipitation, hydrothermal method, followed by modification with chlorin e6 (Ce6)

Dr. S. Yan, Dr. Y. Tang, Prof. Y. Wang, Prof. X. Liu
SZU-NUS Collaborative Center and International Collaborative
Laboratory of 2D Materials for Optoelectronic Science and Technology
of Ministry of Education
Institute of Microscale Optoelectronics
Shenzhen University
Shenzhen 518060, China
E-mail: wangyu@szu.edu.cn; chmlx@nus.edu.sg

Dr. S. Yan
Department of Chemistry
National University of Singapore
Singapore 117543, Singapore

 The ORCID identification number(s) for the author(s) of this article can be found under <https://doi.org/10.1002/adma.201905825>.

DOI: 10.1002/adma.201905825

X. Zeng, Prof. B.-F. Liu
The Key Laboratory for Biomedical Photonics of MOE at Wuhan National
Laboratory for Optoelectronics-Hubei Bioinformatics and Molecular
Imaging Key Laboratory
Systems Biology Theme
Department of Biomedical Engineering
College of Life Science and Technology
Huazhong University of Science and Technology
Wuhan 430074, China
E-mail: bfliu@mail.hust.edu.cn

Prof. Y. Wang
Engineering Technology Research Center for 2D Material Information
Function Devices and Systems of Guangdong Province
Institute of Microscale Optoelectronics
Shenzhen University
Shenzhen 518060, China

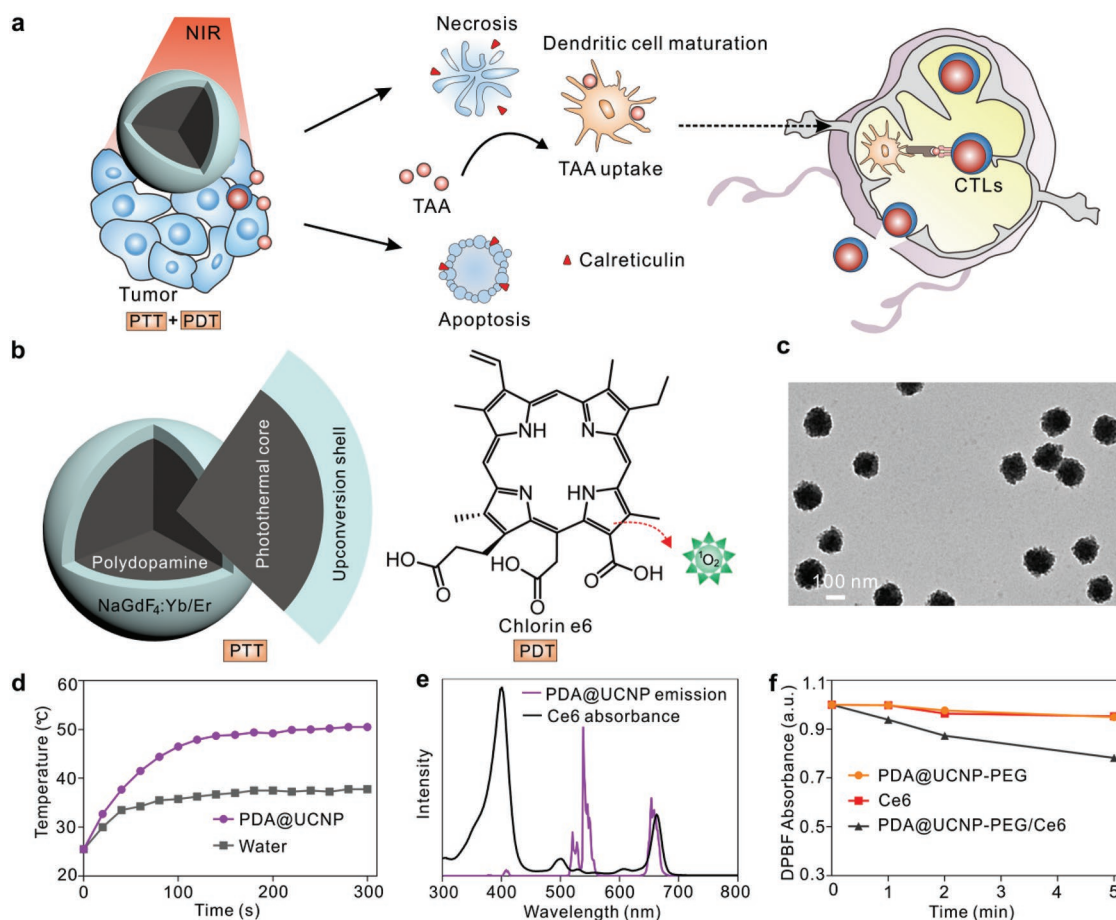


Figure 1. Design and characterization of PDA@UCNP-PEG/Ce6. a) Scheme of synergistic phototherapy for augmentation of antitumor immunity. Upon laser irradiation, designed nanoparticles can ablate the primary tumor through synergistic phototherapy, and the released tumor-associated antigens (TAA) tend to trigger the antitumor immunity which contributes to the inhibition of tumor metastasis and relapse. b) The structure design of core-shell particle, the inner PDA is regarded as the photothermal core for PTT and the upconversion shell is used for PDT through transfer emission light to adsorbed photosensitizer under single 980 nm laser irradiation. c) TEM imaging of the as-prepared PDA@UCNP nanoparticles. d) Temperature profiles of pure water and aqueous dispersions of PDA@UCNP nanoparticles (2 mg mL⁻¹) as a function of irradiation time (0–5 min). e) The spectrum profiles of Ce6 absorption and PDA@UCNP emission excited with a 980 nm laser. f) Comparison of ¹O₂ production of Ce6-unloaded PDA@UCNP-PEG, pure Ce6, and PDA@UCNP-PEG/Ce6 under 980 nm laser irradiation (1 W cm⁻²).

molecules as the photosensitizer. Importantly, this design preserves the photothermal effect of the PDA core for PTT, while simultaneously maximizing the generation of reactive oxygen species (ROS) for PDT. Upon laser irradiation at 980 nm, these core-shell nanoparticles ablate the primary tumor to expose calreticulin protein on the cell membrane. The released antigens during the synergistic phototherapy can trigger the maturation of dendritic cells, which in turn activate cytotoxic T lymphocytes (CTLs) and T memory cells, thereby contributing to the inhibition of tumor metastasis and relapse (Figure 1a).

The particle design for achieving a synergistic effect of combined PTT and PDT was shown in Figure 1b. PDA was selected as the photothermal inner core (Figure S1, Supporting Information) and synthesized through simple self-polymerization in an alkaline solution. We chose PDA as the core to fabricate multifunctional nanomaterials because of its strong absorption in the NIR region, high photothermal conversion ability, and excellent biocompatibility (Figure S1, Supporting Information).^[36–38] The coating of lanthanide (Ln)-doped carbonate hydroxide layer (Gd:Yb,Er(OH)CO₃) onto the PDA core by a urea-mediated coprecipitation method resulted in the formation of PDA@Ln(OH)CO₃ nanoparticles.^[39,40] These particles were then treated with a low concentration of NaF/NH₄F solution to yield PDA@NaGdF₄:Yb/Er nanoparticles (Figure 1c). The as-prepared PDA@UCNPs exhibited the capabilities of photothermal conversion and upconversion emission under 980 nm laser irradiation (Figure 1d,e; Figures S2 and S3, Supporting Information). The high photothermal conversion of PDA@UCNPs was enabled by both the direct absorption of 980 nm

Prof. X. Liu
The N.1 Institute for Health and Department of Chemistry
National University of Singapore
Singapore 117543, Singapore

Prof. X. Liu
Joint School of National University of Singapore and Tianjin University
International Campus of Tianjin University
Fuzhou 350207, P. R. China

laser stimulation and the visible emission through UCNP. We chose Ce6 molecule as the photosensitizer because its absorption largely overlaps with the emission spectrum of PDA@UCNPs. The Ce6 molecules were loaded onto the particles by mixing with multiarm polyethylene glycol (PEG) polymers under magnetic stirring in phosphate buffer solution (PBS) (Figure S4, Supporting Information).^[41,42] Fourier transform infrared (FTIR) spectroscopy showed that the PEG and Ce6 molecules were successfully attached to the particles (Figure S5, Supporting Information). The Ce6 loading capacity was evaluated by UV–vis spectroscopic analysis with the calibration curve of the absorbance at 663 nm, and the results showed that the loading capacity consistently improved upon increasing the feeding mass ratio of Ce6 and PDA@UCNP-PEG (Figure S6, Supporting Information). Also, the PDA@UCNP-PEG/Ce6 showed excellent stability in the PBS (Figure S7, Supporting Information). The change of the upconversion quantum yield from 0.14% for PDA@UCNP to 0.03% for PDA@UCNP-PEG/Ce6 suggests an energy transfer process occurring from PDA@UCNP to Ce6 under 980 nm laser irradiation (Figures S8 and S9, Supporting Information). Moreover, the as-synthesized PDA@UCNP-PEG/Ce6 particles exhibited a quantum yield of 0.06 in singlet oxygen ($^1\text{O}_2$) generation upon 980 nm laser irradiation (Figure S10, Supporting Information). Subsequently, the ability of PDA@UCNP-PEG/Ce6 to generate singlet oxygen ($^1\text{O}_2$) species was evaluated using 1,3-diphenylisobenzofuran as the reporter in solution. As shown in Figure 1f, the PDA@UCNP-PEG/Ce6 could induce intense $^1\text{O}_2$ generation under 980 nm laser excitation. By contrast, no $^1\text{O}_2$ generation could be detected using PDA@UCNP-PEG or Ce6 molecules alone under identical conditions, indicating the utility of our synthetic nanoprobe for PDT.

The PDA@UCNP-PEG/Ce6 nanoprobes showed no apparent toxicity to murine breast 4T1 cancer cell and macrophage RAW164.9 cell at different concentrations for 24 h incubation (Figures S11 and S12, Supporting Information). To confirm the therapeutic performance of synergistic phototherapy, we placed the PDA@UCNP-PEG (with no Ce6 loading) and PDA@UCNP-PEG/Ce6 in an ice bath (elimination of photothermal effect) as PTT and PDT formula, respectively. As shown in Figure S13 of the Supporting Information, under the same light irradiation condition, the PDA@UCNP-PEG/Ce6 group exhibited strong fluorescence intensity in the presence or absence of an ice bath, while the PBS and PDA@UCNP-PEG groups displayed negligible fluorescence by confocal microscopic analysis or flow cytometry measurement. However, without light irradiation, the PDA@UCNP-PEG/Ce6 group could not generate ROS in cells. These results confirmed that the as-prepared PDA@UCNP-PEG/Ce6 nanoprobes possessed a strong capability to kill cancer cells via photodynamic therapy. Subsequently, we further carried out cell apoptosis assay to evaluate the therapeutic outcome of various treatments using Annexin V-FITC/PI kit staining assay and flow cytometry analysis. As shown in Figure S14a,b of the Supporting Information, the blank groups, i.e., PDA@UCNP-PEG/Ce6 or PBS + L (+ L, with light irradiation) groups, caused negligible cytotoxicity. In stark contrast, the cell viability of PDA@UCNP-PEG/Ce6 + L in an ice bath (PDT) and PDA@UCNP-PEG + L (PTT) groups decreased to 77.2% and 34.8%, respectively

(Figure S14c,d, Supporting Information). Strikingly, the cell viability significantly decreased to 25% for PDA@UCNP-PEG/Ce6 + L group (Figure S14e, Supporting Information), suggesting the superior therapeutic outcome of our nanoprobes compared to PDT or PTT alone. Additionally, the PDA@UCNP-PEG/Ce6 + L group could induce the expression of calreticulin on the 4T1 cell membrane (Figure S15, Supporting Information), suggesting the feasibility of triggering immunogenic cell death and adaptive immune response by these nanoprobes.^[29]

We further examined the therapeutic effects of the as-synthesized nanoprobes as an antitumor agent using the 4T1 mouse breast carcinoma model. In a typical experiment, the 4T1 tumor-bearing female BALB/c mice were divided into five groups: PBS with light irradiation (group 1, PBS + L), PDA@UCNP-PEG/Ce6 (group 2), PDA@UCNP-PEG with light irradiation (group 3, PDA@UCNP-PEG + L), and PDA@UCNP-PEG/Ce6 with light irradiation (group 4, PDA@UCNP-PEG/Ce6 + L). Afterward, the mice were intratumorally injected with the assigned schemes, followed by 980 nm laser irradiation of groups 1, 3, and 4 for 5 min. The tumor temperature was recorded by a thermal infrared camera (Figure S16, Supporting Information). The tumor size and body weight were measured every two days after treatment, and the mice were euthanized on day 28 for in situ inspection of tumor weight (Figure 2a–d). We found that the tumor size in group 1 and 2 grew rapidly while group 3 showed a slight tumor inhibition effect. Specifically, the synergistic phototherapy group (group 4) could eradicate the tumors after NIR irradiation. The images of H&E histologic staining and TUNEL immunofluorescent staining of tumor slices showed that more cells death was found in group 4 after treatments (Figure 2e,f; Figure S17, Supporting Information). These results confirmed that synergistic phototherapy had a better performance in tumor ablation than alternative approaches in which PDT or PTT was exercised individually. Also, as shown in Figure S18 of the Supporting Information, there are no obvious damages in major tissues after various treatments, indicating the safety of the as-prepared nanoparticles for tumor treatment.

In another assay, the 4T1 tumor-bearing mice were euthanized on day 24 (14 days after various treatments) for immunological responses analysis via flow cytometry. As shown in Figure 2g,h, mice in group 3 showed significantly enhanced maturation of dendritic cells than the controls (group 1 and 2), demonstrating that the thermal treatment could boost dendritic cell maturation in the tumor-draining lymph node. Significantly, the group 4 had the highest cell maturation efficacy. We further checked the CTLs in the spleen after the treatments. It was found that there were more CTLs upon laser irradiation of PDA@UCNP-PEG/Ce6 (Figure 2i,j). The cytokine levels in serum were also detected and shown in Figure S19 of the Supporting Information. The higher concentration of the IL-6, MCP-1, IFN- λ , TNF- α , and IL-12p70 detected in the PDA@UCNP-PEG/Ce6 plus laser treatment group demonstrated robust activation of humoral immunity, while the lower IL-10 level indicated decreased immunosuppressive M2 macrophages. Taken together, these results indicate that the synergistic phototherapy enabled by PDA@UCNP-PEG/Ce6 could trigger robust antitumor T-cell immune responses and concurrently dampen the immunosuppression.^[43]

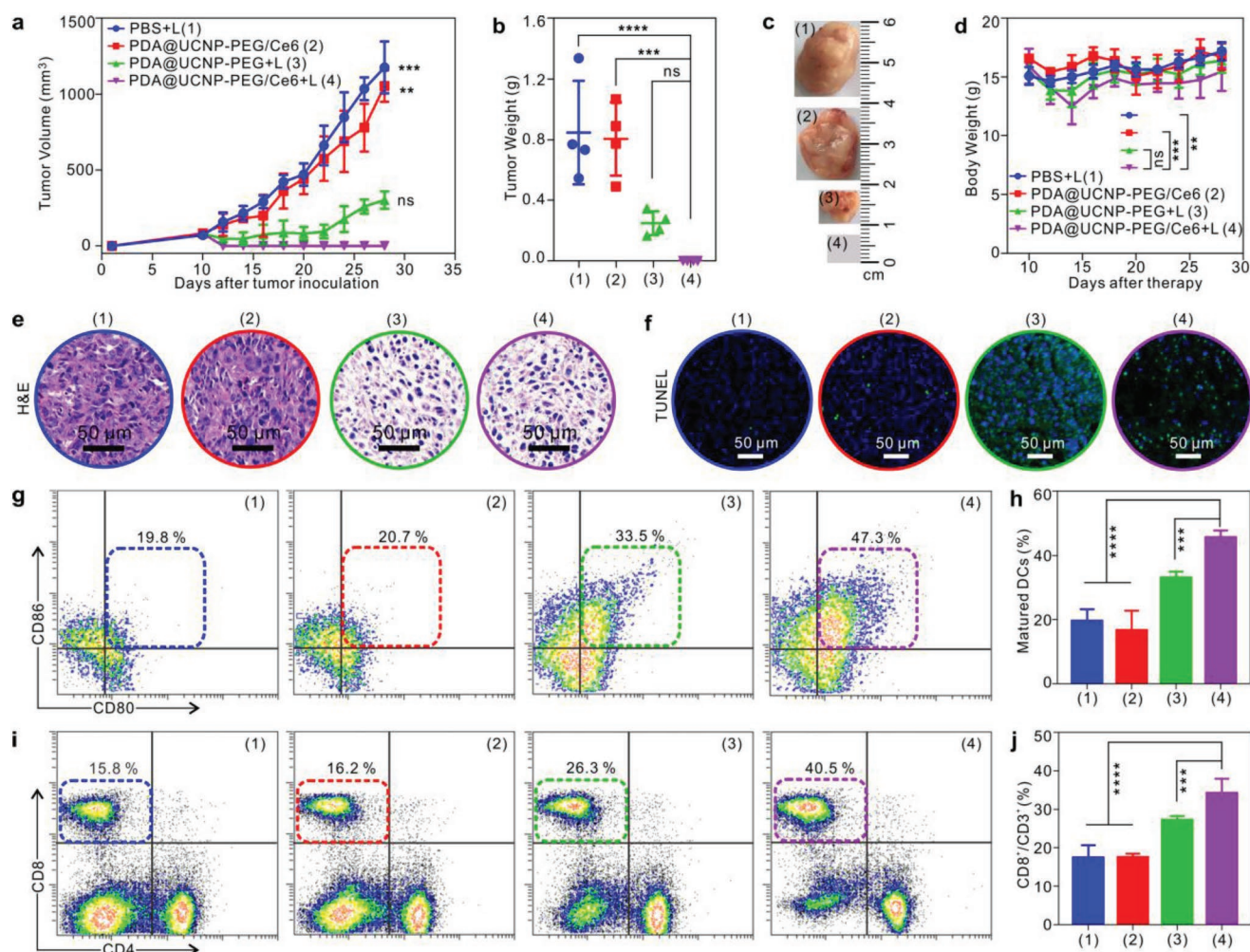


Figure 2. In vivo tumor eradication and antitumor immune response achieved by synergistic phototherapy with PDA@UCNP-PEG/Ce6. a) Tumor growth curve of 4T1 tumor-bearing mice with various treatments. b,c) Weight (b) and representative images (c) of the tumor from each group after euthanizing the animal on day 28. d) Bodyweight of mice over time to the various treatments. e,f) Representative H&E staining (e) and CLSM images of tumors after TUNEL staining (f). g–j) Flow cytometry determination of DC maturation (CD80⁺CD86⁺ gated on CD11c⁺) in tumor-draining lymph node (g,h) and CTLs (CD4⁺CD8⁺ gated on CD3⁺) in the spleen (i,j) from each group on day 24 (14 days after treatment). (e,f) The scale bars are 50 μ m. (a,b,d) $n = 4$; (g,h) $n = 5$; *** $P < 0.001$, **** $P < 0.0001$ and ns: not significant ($p > 0.05$), analyzed by one-way ANOVA, followed by Dunnett's multiple comparisons test. Data represent mean \pm s.d.

As a promising weapon against cancer, immune checkpoint blockade-based therapy, which uses inhibitor molecules to modulate regulatory pathways in T cell costimulatory mechanisms, has led to impressive clinical advances.^[44,45] Specifically, the programmed death 1 (PD-1) pathway has shown effective in impeding the activation of T cell receptors and potentially compromised the therapy outcomes. Thus, the use of inhibitors to blockade the PD-1 pathway for recovered antitumor immune response represents a new generation of cancer treatment. We further examined the efficacy of combining PDA@UCNP-PEG/Ce6 nanoprobe with PD-1 blockade antibody in tumor metastasis inhibition. In this assay, BALB/c mice were subcutaneously inoculated with 4T1 cells and intravenously injected with firefly luciferase-expressed 4T1 (fLuc-4T1) cells on day 8. Two days later, tumor-bearing mice were treated with indicated formulas in the following days (Figure 3a). We treated the mice with five groups:

PBS with light irradiation (PBS + L), PDA@UCNP-PEG/Ce6 (Probe), PDA@UCNP-PEG/Ce6 with light irradiation (Probe + L), PDA@UCNP-PEG/Ce6 with PD-1 (Probe + PD-1), and PDA@UCNP-PEG/Ce6 with light irradiation and PD-1 (Probe + L + PD-1). The primary tumor volume and body weight were recorded every other day after various treatments (Figure 3b; Figure S20, Supporting Information). The survival rates were determined by counting the natural death or the maximum volume (2000 mm³) of the primary tumors (Figure 3c,d). From these results, we can conclude that most of the mice in the Probe + L + PD-1 group could survive up to 100 days after tumor inoculation, and the survival rate reached as high as $\approx 77.8\%$, which was much higher than that of the control groups. However, the Probe + L group (without PD-1 antibody treatment) could only eradicate the primary solid tumors and prolong the survival time to a certain extent, but unfortunately did not protect mice from death caused by tumor

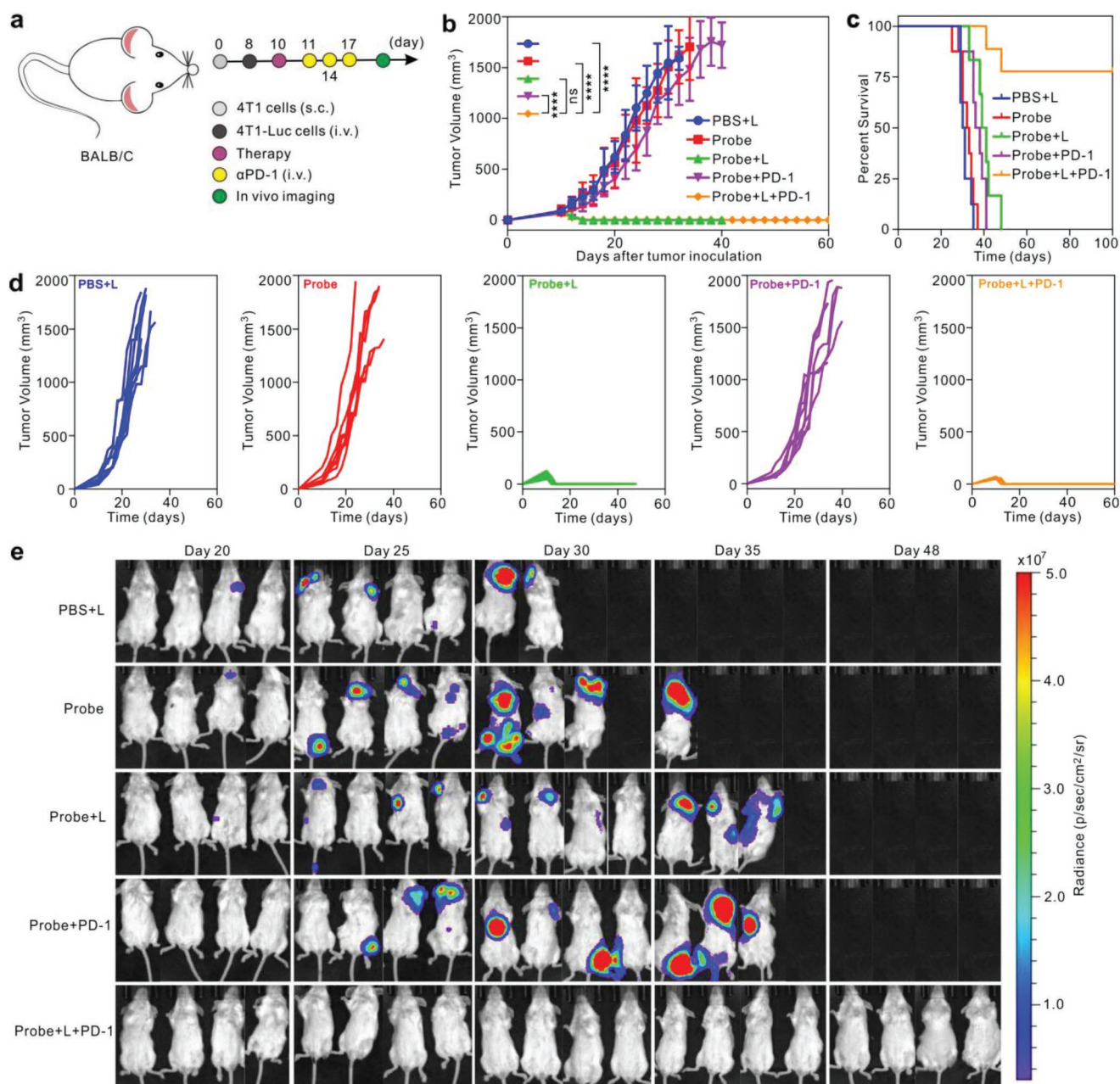


Figure 3. Antitumor efficacy of synthetic probe-based PDT/PTT combined with immune checkpoint blockades. a) BALB/c mice were subcutaneously (s.c.) inoculated with 5×10^5 4T1 cells on day 0 and intravenously (i.v.) injected with 2×10^5 fLuc-4T1 cells on day 8. On day 10, tumor-bearing mice were treated with PBS and the probe with or without laser irradiation. On days 11, 14, and 17, these mice were i.v. injected with α PD-1 antibody (PD-1). b) Average tumor growth kinetics of the mice upon various treatments. Note that the probe in the figure caption refers to PDA@UCNP-PEG/Ce6 nanoparticle. c) Corresponding survival percentages calculated for the mice upon different treatments. d) Individual tumor growth curves of the mice shown in (b). e) In vivo bioluminescence imaging of the i.v. injected fLuc-4T1 cancer cells in different groups upon treatment of the primary tumor. Four representative mice out of 8 to 9 mice per treatment group were shown.

invasion. These results suggest that although the synergistic phototherapy could induce an immune response, the activation and effector functions of CTLs is largely controlled by the immune checkpoints.^[46] Thus, the cooperative phototherapy could not effectively inhibit the growth and spread of intravenously injected fLuc-4T1 cells, as recorded by bioluminescence imaging. As shown in Figure 3e, except for the mice in

the group of Probe + L + PD-1, varying degrees of tumorigenesis and deteriorated tumor metastasis in the mice body were found in the control groups over time. The H&E and India ink stained images of the whole lung tissues (Figure S21, Supporting Information) further confirmed that our fabricated nanoprobe in combination with immune checkpoint blockade could effectively inhibit the tumor metastasis.

We further evaluated the mechanism of the antitumor immune response initiated by synergistic phototherapy and immune checkpoint blockade. The same experimental design as metastasis inhibition assay was used, except without fLuc-4T1 cell injection. After treatment for 25 days, these mice were euthanized, and the spleen, lymph nodes, and blood were harvested for analysis of immune cell markers or cytokines. We found that there were a large number of CTLs, interferon- λ (IFN- λ) expressed CD4 and CD8 cells, and macrophages in the spleen upon treatment with synergistic phototherapy plus PD-1 antibody (Figure 4a–c,h). IFN- λ ⁺CD4⁺ and IFN- λ ⁺CD8⁺ cells also increased in tumor lymph nodes (Figure 4e,f) after treatments. Besides, regulatory T cells (Treg) decreased in both spleen tissues and lymph nodes (Figure 4d,g). The

B cells, which mature in the bone marrow and migrate through the blood to secondary lymphoid organs including the spleen, could present antigen and secrete cytokines.^[47] The increase in the number of the B cells in the spleen after treatment (Figure 4i) also indicated that synergistic phototherapy plus PD-1 induced a systemic immune response required for the activation of cancer immunotherapy. As demonstrated by the previous reports, the upgraded effector memory T cells after tumor therapy could be regarded as an indicator for long-lasting immune response.^[25,27] As shown in Figure 4j, the mice in the group of Probe + L + PD-1 had a higher effector memory T cell ratio compared to other groups. These data support the fact that synergistic phototherapy plus PD-1 can inhibit the tumor relapse and metastasis and thus prolong the

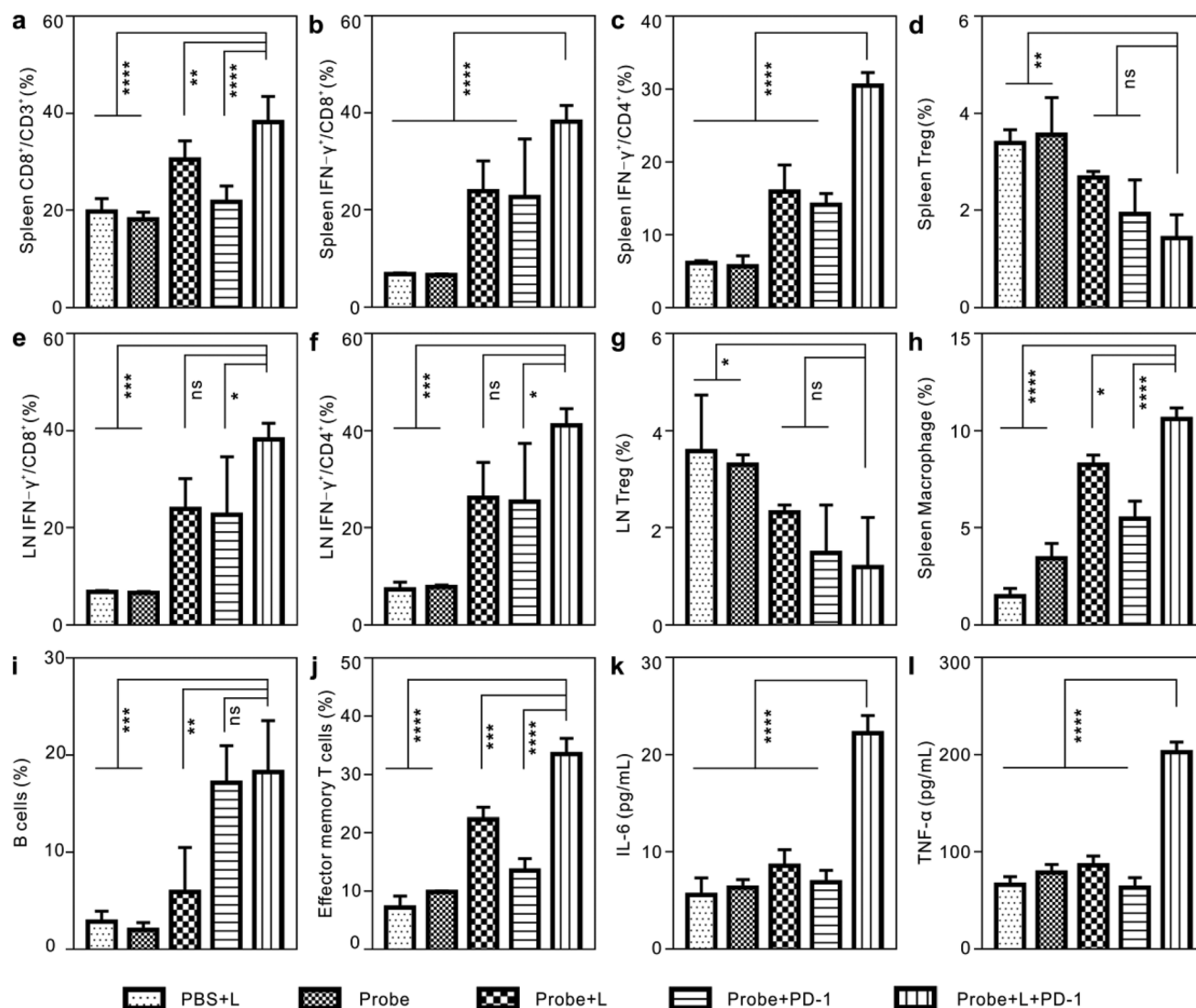


Figure 4. The mechanism of antitumor immunity response initiated by synergistic phototherapy plus immune checkpoint blockade. a–d) Frequencies of CTLs (a, CD4⁺CD8⁺ gated on CD3⁺), IFN- λ ⁺ CD8⁺ cells (b), IFN- λ ⁺ CD4⁺ cells (c), and regulatory T cells (d, CD4⁺FOXP3⁺ gated on CD3⁺) in spleen tissues. e–g) Frequencies of IFN- λ ⁺CD8⁺ cells (e), IFN- λ ⁺CD4⁺ cells (f), and regulatory T cells (g) in lymph nodes. h) Macrophage (b, CD11b⁺F4/80⁺ in spleen cells). i) B cells (B220⁺ gated on CD45⁺CD3⁺). j) Effector memory T cells (d, CD44⁺CD62⁺ gated on CD8⁺CD11b⁺) in the spleen tissues after various treatments for 25 days. k,l) The cytokines IL-6 (k) and TNF- α (l) in serum. * P < 0.05, ** P < 0.01, *** P < 0.001, **** P < 0.0001, and ns: not significant (p > 0.05), analyzed by one-way ANOVA, followed by Dunnett's multiple comparisons test. Data represent mean \pm s.d.

survival time of mice. The significant increment of IL-6 and TNF- α levels in serum further suggested the robust antitumor immune response triggered by our probe with PD-1 blockade (Figure 4k,l).^[48] The representative gating strategies of flow cytometry for T cell detection were shown in Figures S22 and S23 of the Supporting Information.

We also used the bilateral tumor model to test tumor metastasis inhibition. In a typical experiment, one hind leg of the BALB/c mouse was inoculated subcutaneously with B16F10 cells to form primary tumors, and then subcutaneously injected with B16F10 cells at another hind leg flank on day 7 to obtain new tumors. Two days later, only the primary tumors of the mouse were treated with different formulas and injection of PD-1 antibody in the following days (Figure S24a, Supporting Information). According to these results shown in Figure S24b–f of the Supporting Information, we can see that the primary tumors of the mouse were eradicated upon nanoparticle-based phototherapy and the growth of untreated distal tumors was also effectively delayed upon the combination of PD-1 antibody. Intriguingly, even without PD-1 blockades, two mice (out of 6) in the Probe + L group survived up to 60 days, which was probably attributed to the fact that synergistic phototherapy itself could initiate robust systemic immune responses and activate immunotherapy for inhibition of untreated tumors to a certain extent (Figure S24c, Supporting Information). In stark contrast, the growth of both the primary and secondary tumors in the other groups (i.e., PBS + L, Probe, and Probe + PD-1) was totally out of control, and all the mice died within 40 days. Importantly, our synthetic nanoprobe showed excellent biocompatibility (Figures S25–S28, Supporting Information) and long half-life (4.062 h) in the body (Figure S29, Supporting Information). Also, owing to the T1 signal enhancement ability of the Gd element, the probe could also be used for magnetic resonance imaging application (Figure S30, Supporting Information).

Our results provide experimental support for realizing cooperative phototherapy under a single NIR irradiation through the combined use of PDA and UCNPs. The as-prepared core-shell nanoprobe not only obliterate the primary tumor completely but also trigger a robust antitumor immune response. Importantly, our study has shown the feasibility of improving the maturation of dendritic cells and activating CD8⁺ cytotoxic T lymphocytes through the dual-modal phototherapy. This dual-modal phototherapy has also proven effective in recruiting other immunocytes, for instance, the B cells and macrophages. The integration of these nanoprobe with immune checkpoint blockades leads to tumor metastasis inhibition and disseminated tumor suppression with high efficacy. This dual-modal phototherapy can also boost memory T cell activation, which is essential for the prevention of tumor relapse. Our study sheds light on the immunological aspects of combinatorial phototherapy and broadens the scope of synergistic phototherapy-based antitumor immunity, tumor metastasis suppression, and relapse prevention.^[49]

Experimental Section

The experimental details are provided in the Supporting Information.

Supporting Information

Supporting Information is available from the Wiley Online Library or from the author.

Acknowledgements

S.Y. and X.Z. contributed equally to this work. The authors acknowledge the support from the National Natural Science Foundation of China (Grant Nos. 61705137, 61805153, and 21775049), China Postdoctoral Science Foundation (2018M643174), the Science and Technology Project of Shenzhen (Grant Nos. JCY20170817093821657, KQJSCX20180328093614762, and ZDSYS201707271014468), the Educational Commission of Guangdong Province (Grant No. 2016KCXTD006), the Singapore Ministry of Education (MOE2017-T2-2-110), Agency for Science, Technology and Research (A*STAR) (Grant No. A1883c0011), National Research Foundation, Prime Minister's Office, Singapore under its Competitive Research Program (Award No. NRF-CRP15-2015-03), and under the NRF Investigatorship programme (Award No. NRF-NRFI05-2019-0003). The authors thank Z. Luo and Dr. Z. Li for helpful discussion, and thank Dr. L. Liang for upconversion quantum yield measurement.

Conflict of Interest

The authors declare no conflict of interest.

Keywords

immunotherapy, metastasis inhibition, synergistic phototherapy, upconversion

Received: September 6, 2019
Published online: September 30, 2019

- [1] C. M. J. Hu, L. Zhang, *Biochem. Pharmacol.* **2012**, *83*, 1104.
- [2] W. Fan, B. Yung, P. Huang, X. Chen, *Chem. Rev.* **2017**, *117*, 13566.
- [3] Q. Xiao, X. Zheng, W. Bu, W. Ge, S. Zhang, F. Chen, H. Xing, Q. Ren, W. Fan, K. Zhao, Y. Hua, J. Shi, *J. Am. Chem. Soc.* **2013**, *135*, 13041.
- [4] T. H. Tran, R. K. Thapa, H. T. Nguyen, T. T. Pham, T. Ramasamy, D. S. Kim, C. S. Yong, J. O. Kim, H. Choi, *J. Pharm. Invest.* **2016**, *46*, 505.
- [5] J. Oh, H. Yoon, J. H. Park, *Biomed. Eng. Lett.* **2013**, *3*, 67.
- [6] L. Cheng, C. Wang, L. Feng, K. Yang, Z. Liu, *Chem. Rev.* **2014**, *114*, 10869.
- [7] F. Wang, Y. Han, C. S. Lim, Y. Lu, J. Wang, J. Xu, H. Chen, C. Zhang, M. Hong, X. Liu, *Nature* **2010**, *463*, 1061.
- [8] N. M. Idris, M. K. Gnanasamandhan, J. Zhang, P. C. Ho, R. Mahendran, Y. Zhang, *Nat. Med.* **2012**, *18*, 1580.
- [9] G. Chen, H. Qiu, P. N. Prasad, X. Chen, *Chem. Rev.* **2014**, *114*, 5161.
- [10] R. Lv, P. Yang, F. He, S. Gai, C. Li, Y. Dai, G. Yang, J. Lin, *ACS Nano* **2015**, *9*, 1630.
- [11] D. Yang, P. Ma, Z. Hou, Z. Cheng, C. Li, J. Lin, *Chem. Soc. Rev.* **2015**, *44*, 1416.
- [12] S. Han, A. Samanta, X. Xie, L. Huang, J. Peng, S. J. Park, D. B. L. Teh, Y. Choi, Y. T. Chang, Y. Yang, B. Xing, X. Liu, *Adv. Mater.* **2017**, *29*, 1700244.
- [13] S. Chen, A. Z. Weitemier, X. Zeng, L. He, X. Wang, Y. Tao, A. J. Y. Huang, Y. Hashimoto, M. Kano, H. Iwasaki,

- L. K. Parajuli, S. Okabe, D. B. Teh, A. H. All, I. Tsutsui-Kimura, K. F. Tanaka, X. Liu, T. J. McHugh, *Science* **2018**, 359, 679.
- [14] B. Zhou, B. Shi, D. Jin, X. Liu, *Nat. Nanotechnol.* **2015**, 10, 924.
- [15] L. Liang, D. B. Teh, N.-D. Dinh, W. Chen, Q. Chen, Y. Wu, S. Chowdhury, A. Yamanaka, T. C. Sum, C.-H. Chen, N. V. Thakor, A. H. All, X. Liu, *Nat. Commun.* **2019**, 10, 1391.
- [16] X. Zeng, S. Chen, A. Weitemier, S. Han, A. Blasiak, A. Prasad, K. Zheng, Z. Yi, B. Luo, I. H. Yang, N. Tarkor, C. Chai, K.-L. Lin, T. J. McHugh, A. H. All, X. Liu, *Angew. Chem., Int. Ed.* **2019**, 58, 9262.
- [17] Z. Yi, Z. Luo, N. D. Barth, X. Meng, H. Liu, W. Bu, A. M. All, X. Liu, *Adv. Mater.* **2019**, 31, 1901851.
- [18] X. Qin, J. Xu, Y. Wu, X. Liu, *ACS Cent. Sci.* **2019**, 5, 29.
- [19] A. P. Castano, P. Mroz, M. R. Hamblin, *Nat. Rev. Cancer* **2006**, 6, 535.
- [20] P. Agostinis, K. Berg, K. A. Cengel, T. H. Foster, A. W. Girotti, S. O. Gollnick, S. M. Hahn, M. R. Hamblin, A. Juzeniene, D. Kessel, M. Korbelik, J. Moan, P. Mroz, D. Nowis, J. Piette, B. C. Wilson, J. Golab, *Ca-Cancer J. Clin.* **2011**, 61, 250.
- [21] B. Ding, S. Shao, C. Yu, B. Teng, M. Wang, Z. Cheng, K. L. Wong, P. Ma, J. Lin, *Adv. Mater.* **2018**, 30, 1802479.
- [22] G. Kroemer, L. Galluzzi, O. Kepp, L. Zitvogel, *Annu. Rev. Immunol.* **2013**, 31, 51.
- [23] J. Xu, L. Xu, C. Wang, R. Yang, Q. Zhuang, X. Han, Z. Dong, W. Zhu, R. Peng, Z. Liu, *ACS Nano* **2017**, 11, 4463.
- [24] W. Song, J. Kuang, C. Li, M. Zhang, D. Zheng, X. Zeng, C. Liu, X. Zhang, *ACS Nano* **2018**, 12, 1978.
- [25] K. Lu, C. He, N. Guo, C. Chan, K. Ni, G. Lan, H. Tang, C. Pelizzari, Y. X. Fu, M. T. Spiotto, R. R. Weichselbaum, W. Lin, *Nat. Biomed. Eng.* **2018**, 2, 600.
- [26] R. Kuai, W. Yuan, S. Son, J. Nam, Y. Xu, Y. Fan, A. Schwendeman, J. J. Moon, *Sci. Adv.* **2018**, 4, eaao1736.
- [27] W. Jiang, C. A. von Roemeling, Y. Chen, Y. Qie, X. Liu, J. Chen, B. Y. S. Kim, *Nat. Biomed. Eng.* **2017**, 1, 0029.
- [28] C. Wang, Y. Ye, Q. Hu, A. Bellotti, Z. Gu, *Adv. Mater.* **2017**, 29, 1606036.
- [29] M. Obeid, A. Tesniere, F. Ghiringhelli, G. M. Fimia, L. Apetoh, J. L. Perfettini, M. Castedo, G. Mignot, T. Panaretakis, N. Casares, D. Métivier, D. N. Larochette, P. N. Ender, F. Ciccocanti, M. Piacentini, L. Zitvogel, G. Kroemer, *Nat. Med.* **2007**, 13, 54.
- [30] L. Guo, D. D. Yan, D. Yang, Y. Li, X. Wang, O. Zalewski, B. Yan, W. Lu, *ACS Nano* **2014**, 8, 5670.
- [31] S. S. Evans, E. A. Repasky, D. T. Fisher, *Nat. Rev. Immunol.* **2015**, 15, 335.
- [32] Q. Chen, L. Xu, C. Liang, C. Wang, R. Peng, Z. Liu, *Nat. Commun.* **2016**, 7, 13193.
- [33] R. Slovak, J. M. Ludwig, S. N. Gettinger, R. S. Herbst, H. S. Kim, *J. Immuno Ther. Cancer* **2017**, 5, 78.
- [34] J. Nam, S. Son, L. J. Ochyl, R. Kuai, A. Schwendeman, J. J. Moon, *Nat. Commun.* **2018**, 9, 1074.
- [35] C. W. Ng, J. Li, K. Pu, *Adv. Funct. Mater.* **2018**, 28, 1804688.
- [36] H. Lee, S. M. Dellatore, W. M. Miller, P. B. Messersmith, *Science* **2007**, 318, 426.
- [37] W. Qiang, W. Li, X. Li, X. Chen, D. Xu, *Chem. Sci.* **2014**, 5, 3018.
- [38] X. Zhong, K. Yang, Z. Dong, X. Yi, Y. Wang, C. Ge, Y. Zhao, Z. Liu, *Adv. Funct. Mater.* **2015**, 25, 7327.
- [39] X. Zhu, J. Zhou, M. Chen, M. Shi, W. Feng, F. Li, *Biomaterials* **2012**, 33, 4618.
- [40] G. Tian, Z. Gu, X. Liu, L. Zhou, W. Yin, L. Yan, S. Jin, W. Ren, G. Xing, S. Li, Y. Zhao, *J. Phys. Chem. C* **2011**, 115, 23790.
- [41] G. Prencipe, S. M. Tabakman, K. Welsher, Z. Liu, A. P. Goodwin, L. Zhang, J. Henry, H. Dai, *J. Am. Chem. Soc.* **2009**, 131, 4783.
- [42] C. Wang, H. Tao, L. Cheng, Z. Liu, *Biomaterials* **2011**, 32, 6145.
- [43] G. Yang, L. Xu, Y. Chao, J. Xu, X. Sun, Y. Wu, R. Peng, Z. Liu, *Nat. Commun.* **2017**, 8, 902.
- [44] P. Sharma, J. P. Allison, *Science* **2015**, 348, 56.
- [45] A. Ribas, J. D. Wolchok, *Science* **2018**, 359, 1350.
- [46] D. M. Pardoll, *Nat. Rev. Cancer* **2012**, 12, 252.
- [47] M. D. Cooper, *Nat. Rev. Immunol.* **2015**, 15, 191.
- [48] M. H. Spitzer, Y. Carmi, N. E. Reticker-Flynn, S. S. Kwek, D. Madhireddy, M. M. Martins, P. F. Gherardini, T. R. Prestwood, J. Chabon, S. C. Bendall, L. Fong, G. P. Nolan, E. G. Engleman, *Cell* **2017**, 168, 487.
- [49] M. Wang, J. Song, F. Zhou, A. R. Hoover, C. Murray, B. Zhou, L. Wang, J. Qu, W. R. Chen, *Adv. Sci.* **2019**, 6, 1802157.